Electronic Supplementary Material (ESI) for Inorganic Chemistry Frontiers.

Supporting Information

Tunable thermotropic phase transition triggering large dielectric response and superionic conduction in lead halide perovskites

Dong-Sheng Shao,[a] Lei Sang,[a] Ya-Ru Kong,[a] Zheng-Rong Deng,[a] Hong-Bin Luo,*[a] Zheng-Fang Tian,[b] Xiao-Ming Ren*[a,c,d]

[a] State Key Laboratory of Materials-Oriented Chemical Engineering and College of Chemistry and Molecular Engineering, Nanjing Tech University, Nanjing 211816, P. R. China

[b] Hubei Key Laboratory for Processing and Application of Catalytic Materials, Huanggang Normal University, Huanggang 438000, P. R. China

[c] College of Materials Science and Engineering, Nanjing Tech University, Nanjing 211816, P. R. China

[d] State Key Laboratory of Coordination Chemistry, Nanjing University, Nanjing 210093, P. R. China

Tel: 86-25-58139476

E-mail: hbluo@njtech.edu.cn (HBL); xmren@njtech.edu.cn (XMR)

Contents

Figure S1. Experimental and simulated PXRD patterns of **1**−**5**.

Figure S2. TG curves of **1**−**5**.

Figure S3. DSC curves with two sequential heating-cooling runs for (a) **2**, (b) **3**, (c) **4** and (d) **5**.

Figure S4. Variable-temperature PXRD patterns PXRD patterns of (a, b) **2**, (c, d) **3**, (e, f) **4**, (g, h) **5**.

Figure S5. Temperature dependent dielectric permittivity (ε′) at the selected frequencies for (a) **2**, (b) **3**, (c) **4**, (d) **5**.

Figure S6. Morphology of **1** (a) the pristine crystals and (b) the crystals under a glass plate annealed at 503 K for 10 minutes, the gravity of glass plate leads the crystals of **1** to clear deformation.

Figure S7. The electron band structures near the Fermi level for (a) **1** and (b) **5**.

Figure S8. Nyquist plots of **1** at the selected temperatures.

Figure S9. (a–c) Nyquist plots of **2** at the selected temperatures and (d) temperature-dependent ionic conductivity.

Figure S10. (a–c) Nyquist plots of **3** at the selected temperatures and (d) temperature-dependent ionic conductivity.

Figure S11. (a–c) Nyquist plots of **4** at the selected temperatures and (d) temperature-dependent ionic conductivity.

Figure S12. (a–c) Nyquist plots of **5** at the selected temperatures and (d) temperature-dependent ionic conductivity.

Figure S13. The representative impedance spectra (solid circles) together with the fit curves at the selected temperatures for **1**. The theoretic lines were re-produced using the fit parameters, and these parameters were acquired by the equivalent circuit method.

Figure S14. Temperature-dependent ionic conductivity of (a) **2**, (b) **3**, (c) **4**, (d) **5**.

Figure S15. Time-dependent current of **1** at 463 K.

Table S1. Crystallographic date and refinement parameter for **1**−**5** at 100 K

References

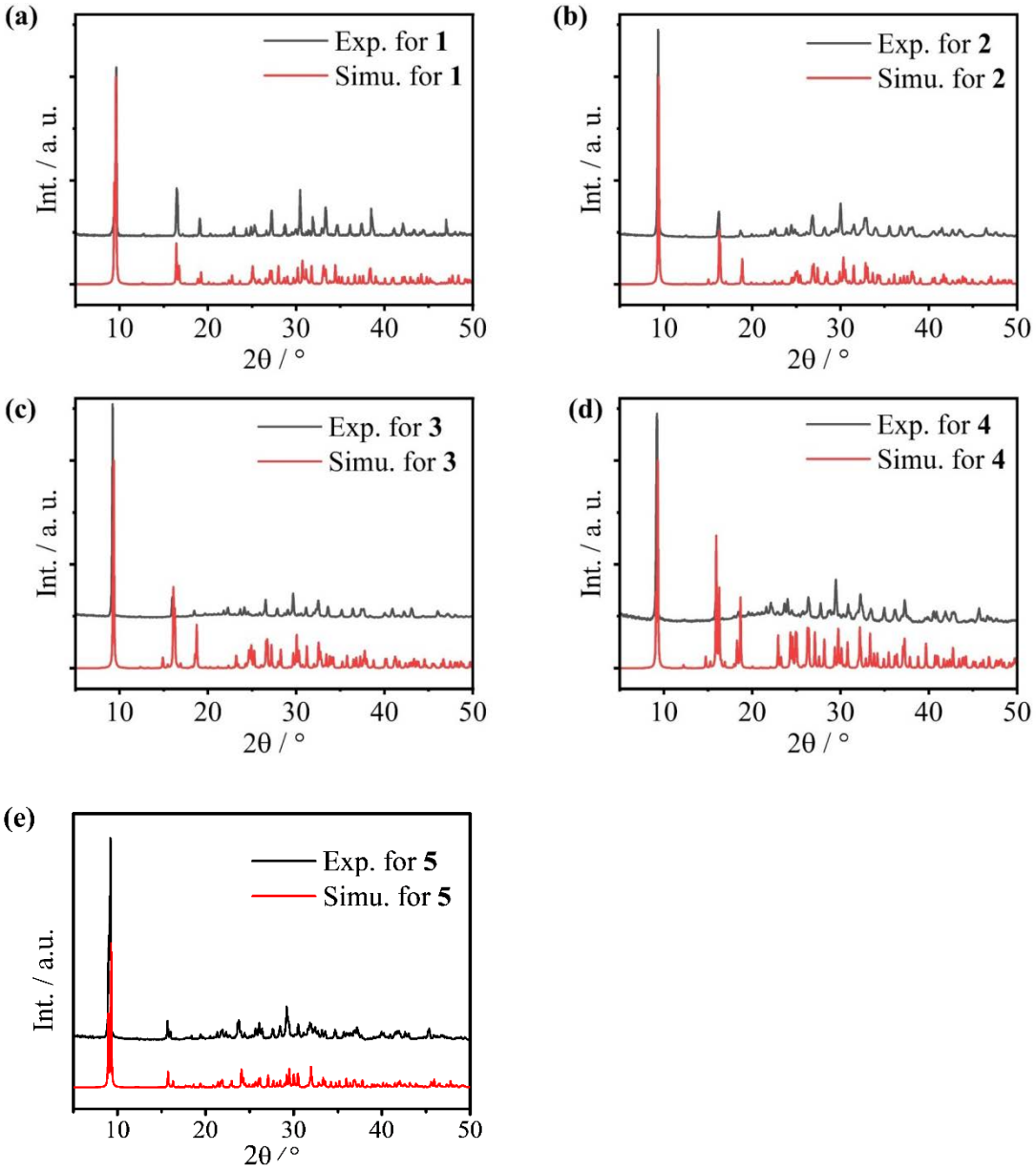

Figure S1. Experimental and simulated PXRD patterns of **1**−**5**.

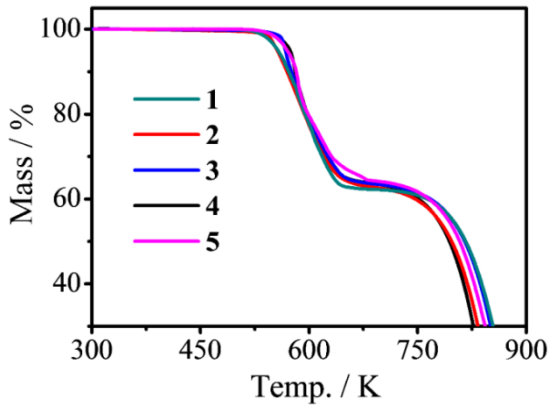

Figure S2. TG curves of **1**−**5**.

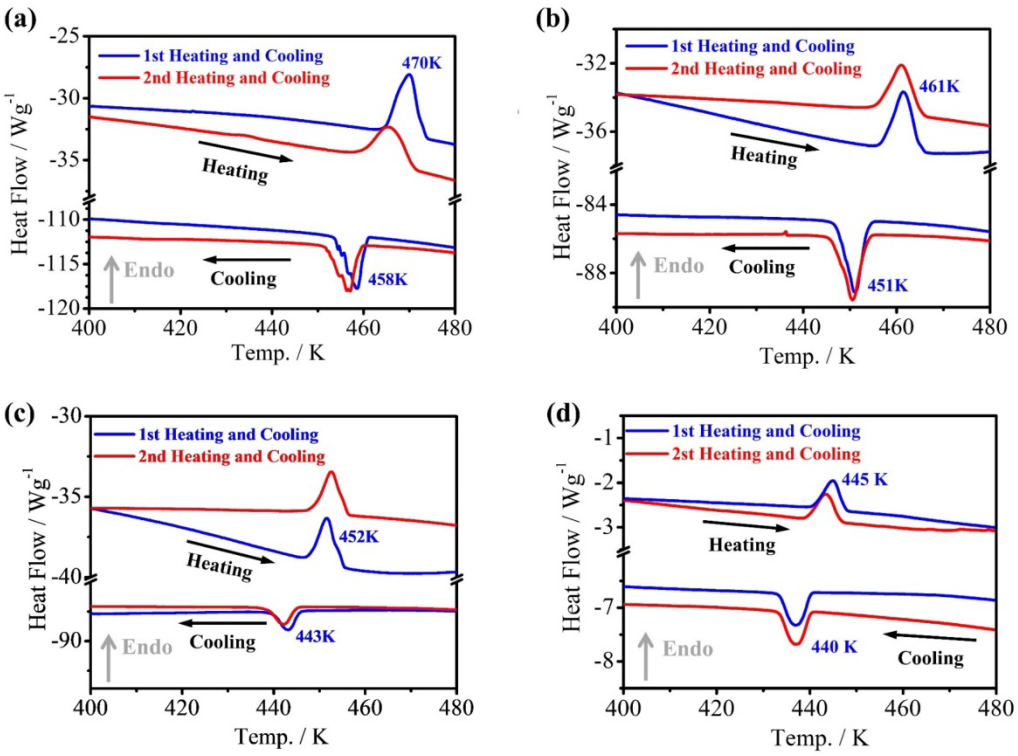

Figure S3. DSC curves with two sequential heating-cooling runs for (a) **2**, (b) **3**, (c) **4** and (d) **5**.

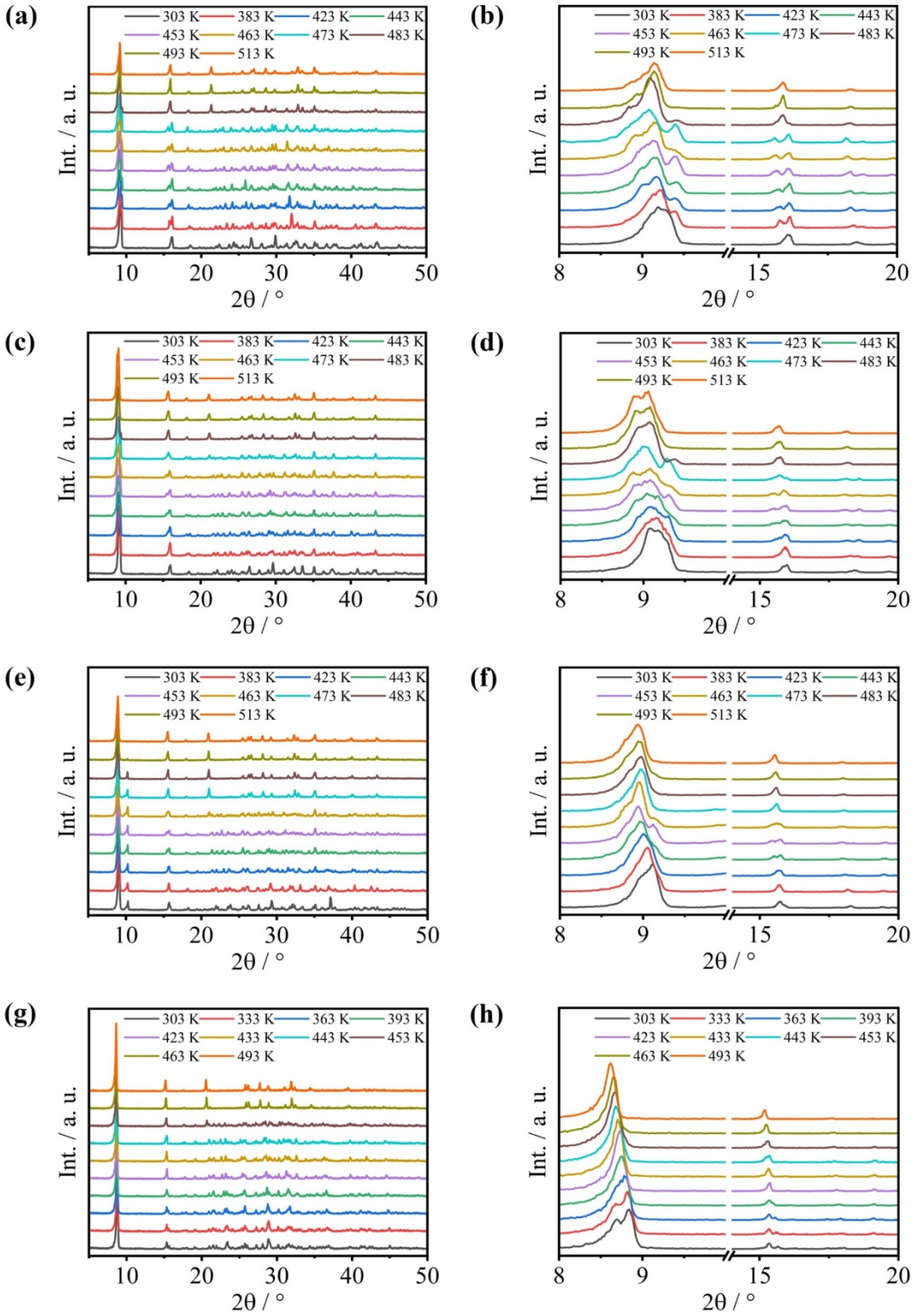

Figure S4. Variable-temperature PXRD patterns PXRD patterns of (a, b) **2**, (c, d) **3**, (e, f) **4**, (g, h) **5**.

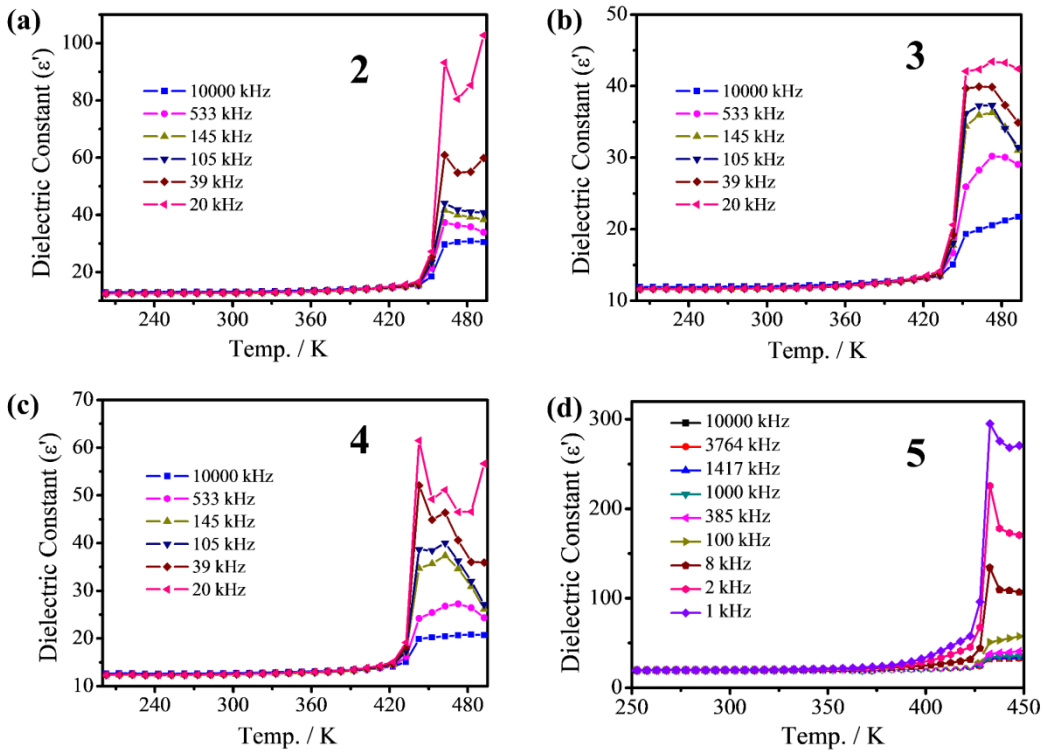

Figure S5. Temperature dependent dielectric permittivity (ε′) at the selected frequencies for (a) **2**, (b) **3**, (c) **4**, (d) **5**.

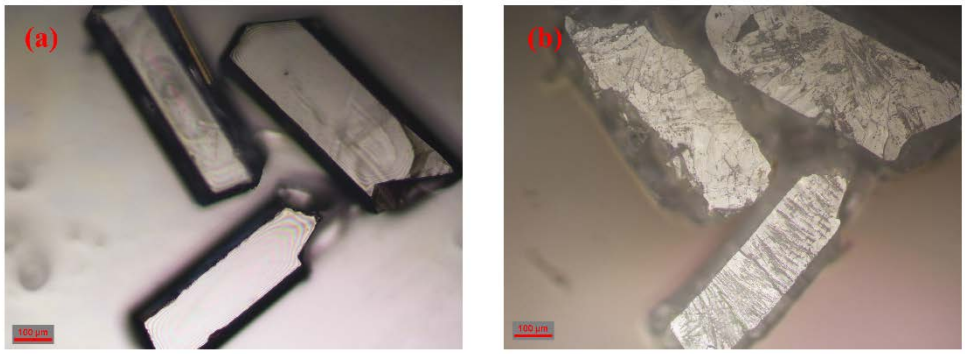

Figure S6. Morphology of **1** (a) the pristine crystals and (b) the crystals under a glass plate annealed at 503 K for 10 minutes, the gravity of glass plate leads the crystals of **1** to clear deformation.

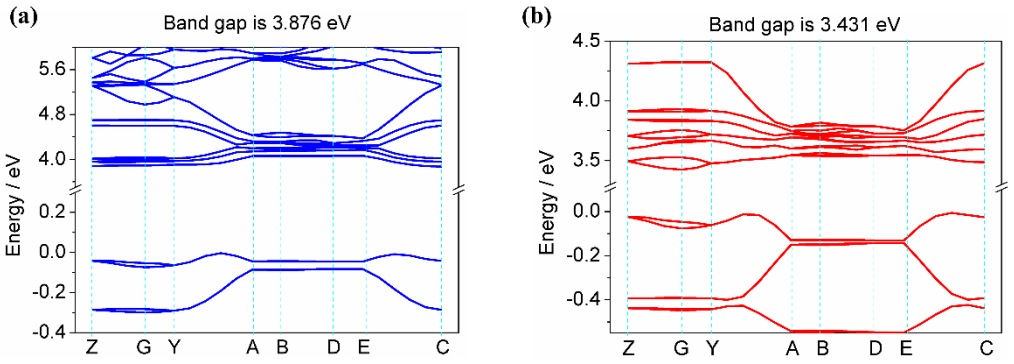

Figure S7. The electron band structures near the Fermi level for (a) **1** and (b) **5**, and the k-points correspond to Z (0, 0, 0.5), G (0, 0, 0), Y (0, 0.5, 0), A (–0.5, 0.5, 0), B(–0.5, 0, 0), D(–0.5, 0, 0.5), E(–0.5, 0.5, 0.5) and C (0, 0.5, 0.5).

The electron band structure, density of states (DOS) and projected density of states (PDOS) were calculated for **1** and **5** in the framework of density functional theory (DFT) using the CASTEP module.[1] The crystal structures were directly taken from single crystal structure analysis for **1** and **5**. The total plane-wave pseudopotential method forms the basis of the CASTEP calculations. The exchange–correlation effects were treated within the generalized gradient approximation (GGA) with the Perdew–Burke–Ernzerhof (PBE) functional.[2] The cut-off energy was set at 517 eV for the plane wave basis. All other calculation parameters were set at the default values in the CASTEP code.

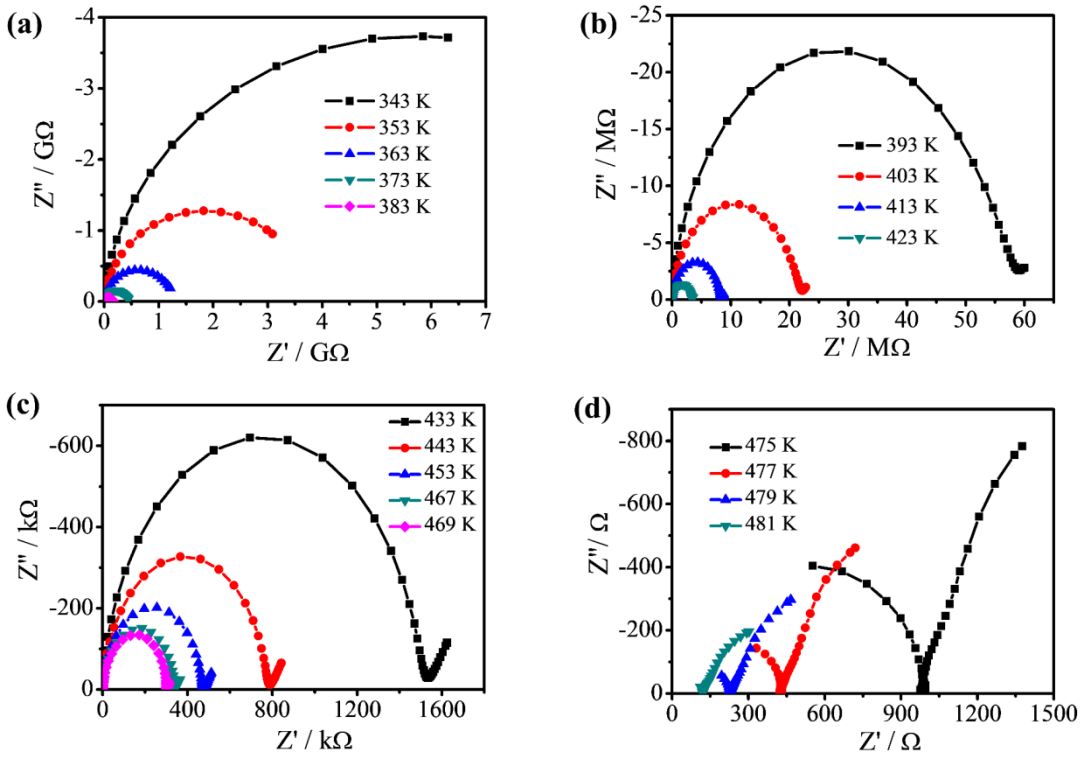

Figure S8. Nyquist plots of **1** at the selected temperatures.

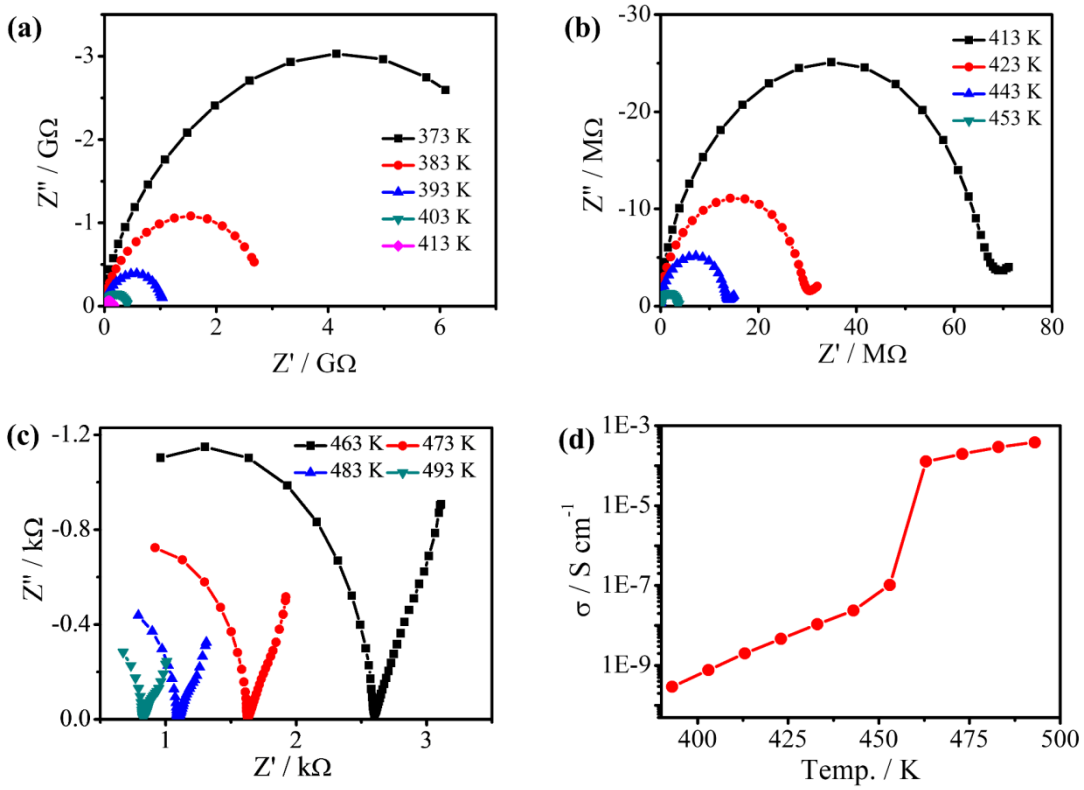

Figure S9. (a–c) Nyquist plots of **2** at the selected temperatures and (d) temperature-dependent ionic conductivity.

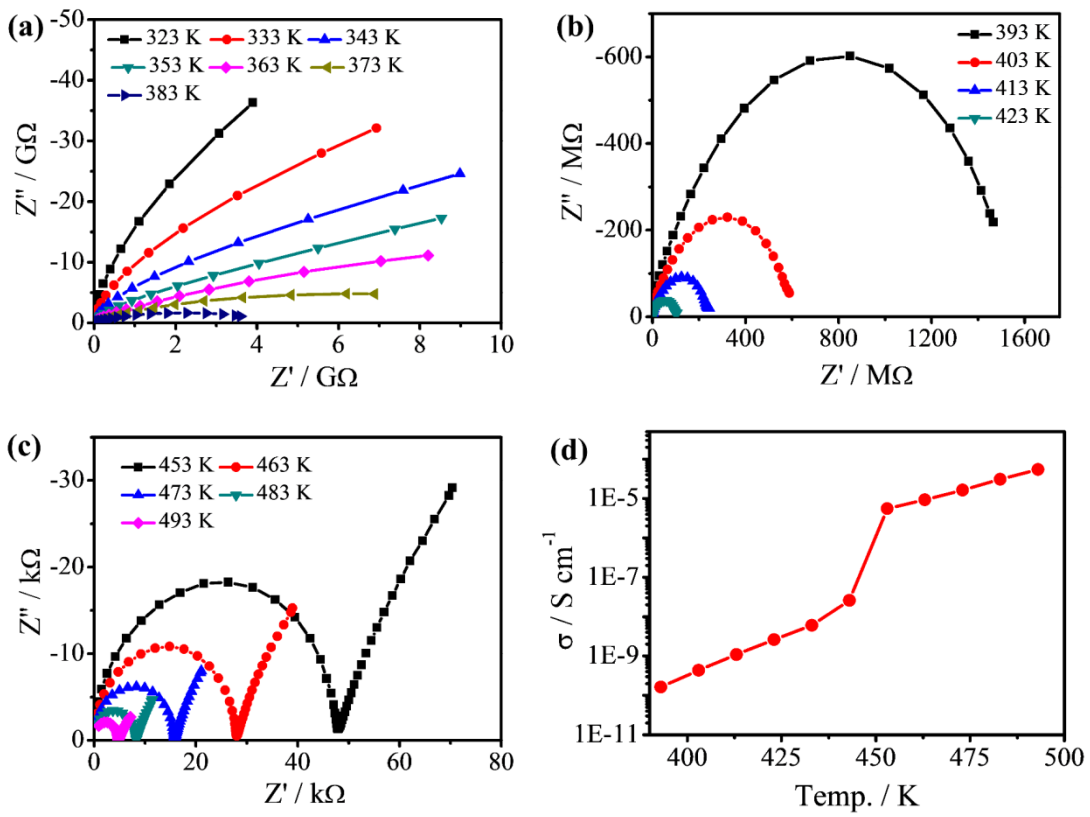

Figure S10. (a–c) Nyquist plots of **3** at the selected temperatures and (d) temperature-dependent ionic conductivity.

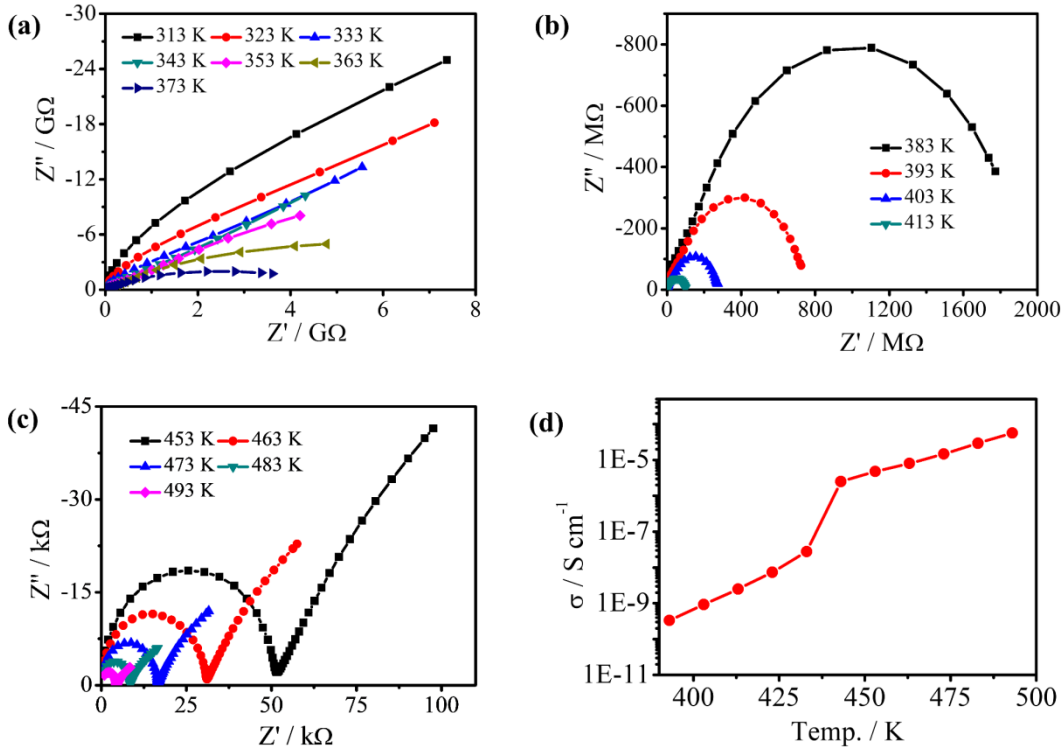

Figure S11. (a–c) Nyquist plots of **4** at the selected temperatures and (d) temperature-dependent ionic conductivity.

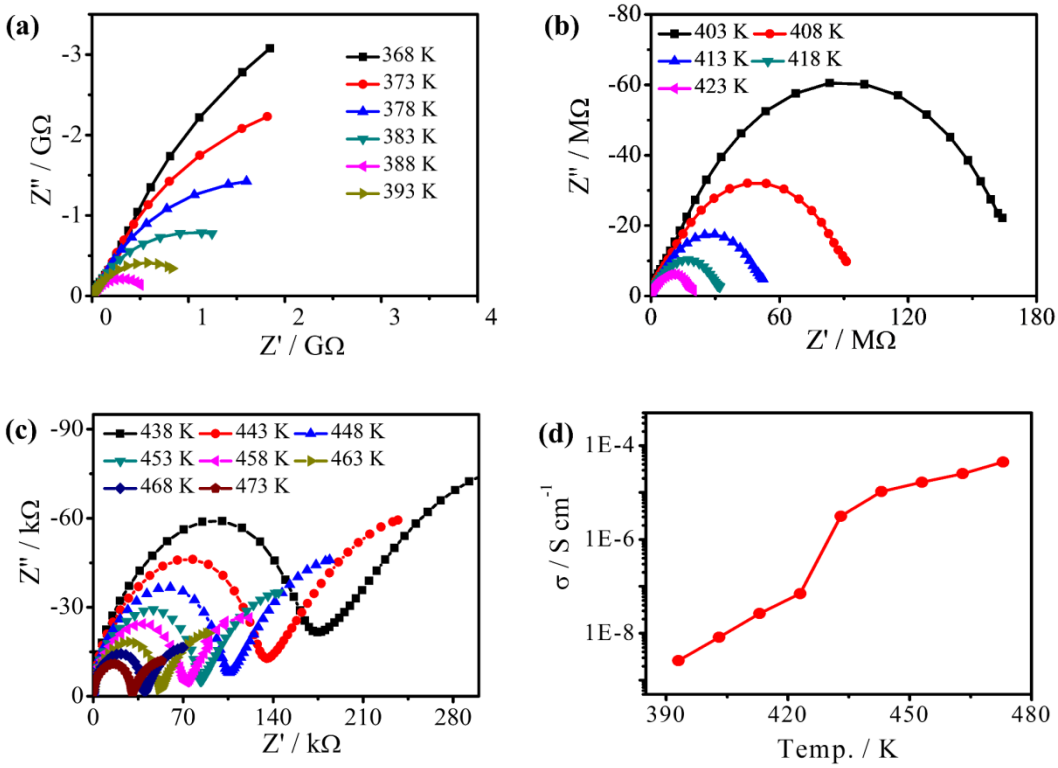

Figure S12. (a–c) Nyquist plots of **5** at the selected temperatures and (d) temperature-dependent ionic conductivity.

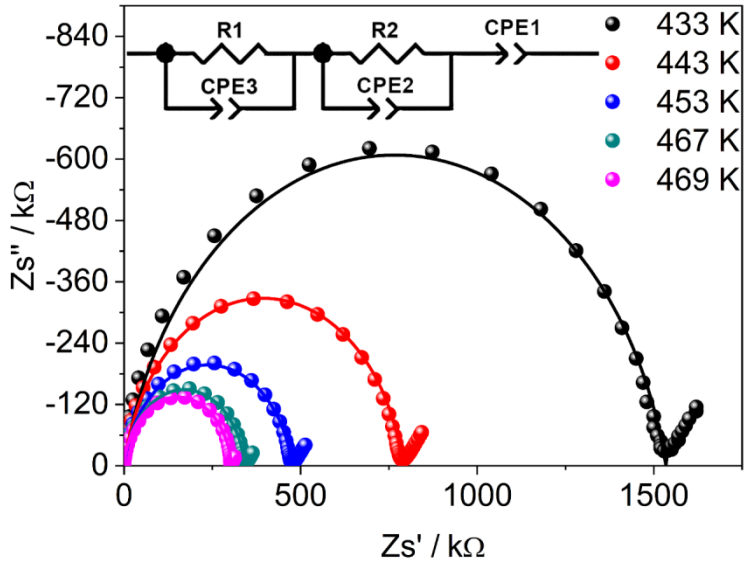

Figure S13. The representative impedance spectra (solid circles) together with the fit curves at the selected temperatures for **1**. The lines are theoretically reproduced plots using fit parameters, which are acquired by the equivalent circuits in the insets.

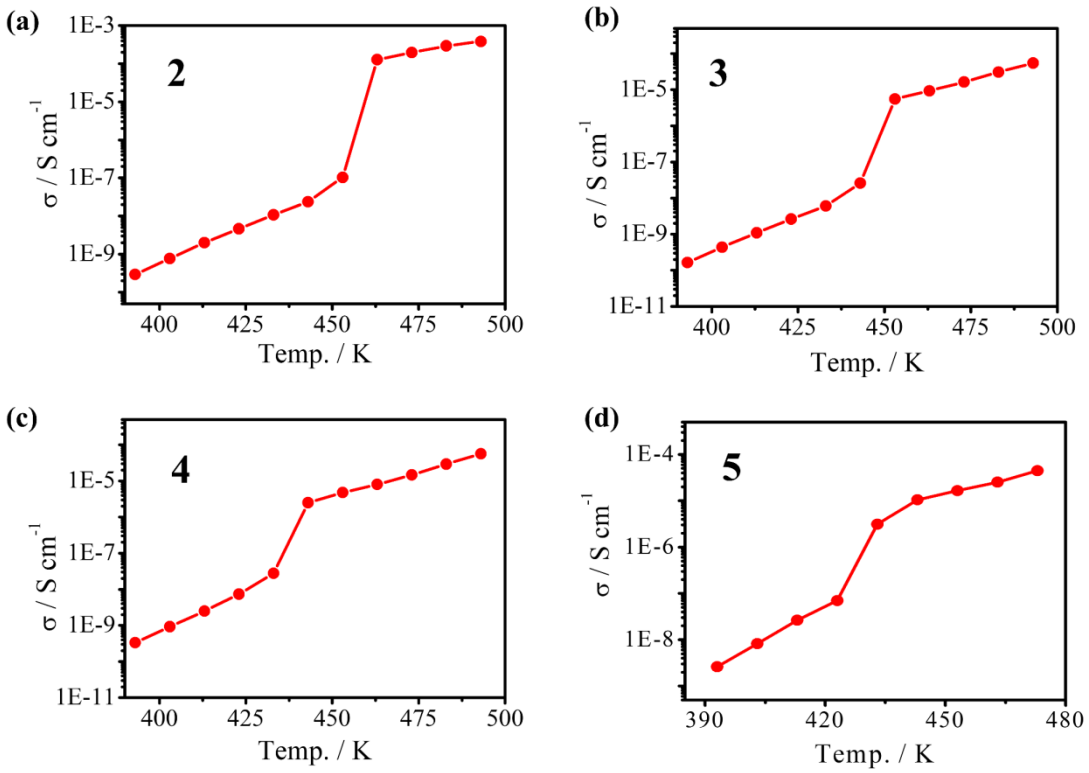

Figure S14. Temperature-dependent ionic conductivity of (a) **2**, (b) **3**, (c) **4**, (d) **5**.

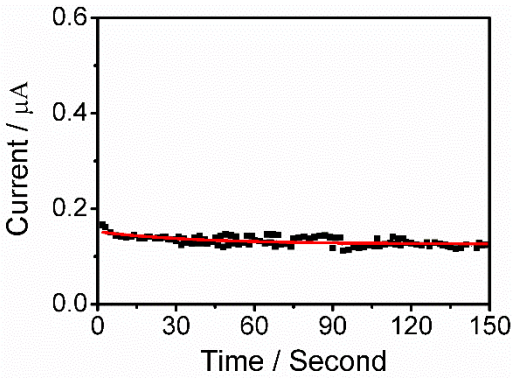

Figure S15. Time-dependent current of **1** at 463 K. The chronoamperometry measurements have been carried out for **1** to evaluate electronic conductivity, the DC voltage is 2 V, the pellet sample of **1** is in the thickness of 1.262 mm and diameter of 7.0 mm. As indicated by the plots of current against time, the current is decreased rapidly within the initial several seconds, then stabilized at a constant value, suggesting the coexistence of ionic and electronic conduction in **1**. The electron current can be acquired by fitting the plots of current against time with the equation of

$I = I_0 + A_0\exp(-\frac{t}{t_0})$, in which I is the total current, I_0 is the electron current, A_0 and t_0 are the constants. Then, the electronic conductivity of **1** is calculated based on the acquired electron current, applied DC voltage and geometric parameters of pellet samples. The electronic conductivity (σ_e) of **1** is calculated to be 2.07×10^{-8} S cm^{-1} at 463 K, which are over 10 times smaller than the conductivity acquired from AC impedance measurements, demonstrating that the conduction of **1** is largely contributed by the ionic conduction.

Table S1. Crystallographic date and refinement parameter for **1**−**5** at 100 K

Compound	**1**	**2**	**3**	**4**	**5**[3]
Formula	$C_9H_{22}NBr_3Pb$	$C_9H_{22}NBr_{1.92}I_{1.08}Pb$	$C_9H_{22}NBr_{1.17}I_{1.83}Pb$	$C_9H_{22}NBr_{0.50}I_{2.50}Pb$	$C_9H_{22}NI_3Pb$
FW	591.20	642.18	677.07	708.91	732.16
CCDC No.	2174164	2174166	2174163	2174165	1535129
Wavelength /Å	0.71073	0.71073	0.71073	0.71073	0.71073
Crystal system	Monoclinic	Monoclinic	Monoclinic	Monoclinic	Monoclinic
SG	$P2_1/c$	$P2_1/n$	$P2_1/n$	$P2_1/n$	$P2_1/c$
a (Å)	7.7006(5)	7.7921(5)	7.8506(5)	7.9355(4)	7.9794(4)
b (Å)	18.7981(11)	18.9126(12)	19.1273(11)	19.3923(10)	19.7234(10)
c (Å)	11.5875(6)	11.2022(7)	11.2807(6)	11.3087(6)	11.8995(5)
α (°)	90.00	90.00	90.00	90.00	90.00
β (°)	113.920(3)	104.955(2)	104.981(2)	105.615(2)	114.079(3)
γ (°)	90.00	90.00	90.00	90.00	90.00
V(Å3) / Z	1533.30(16)	1594.94(18)	1636.34(17)	1676.04(15)	1709.79(15)
ρ (g cm^{-3})	2.561	2.674	2.748	2.809	2.844
F (000)	1080	1158	1212	1260	1296
Abs. coeff. / mm^{-1}	18.793	17.449	16.595	15.835	15.258
θ Range for data col. (°)	2.89-27.53	2.15 -27.54	2.13-27.52	2.10-27.55	2.79-27.516
Index ranges	$-10 \le h \le 10$ $-24 \le k \le 24$ $-15 \le l \le 15$	$-10 \le h \le 9$ $-24 \le k \le 24$ $-14 \le l \le 14$	$-10 \le h \le 10$ $-24 \le k \le 24$ $-14 \le l \le 14$	$10 \le h \le 10$ $-25 \le k \le 25$ $-14 \le l \le 13$	$10 \le h \le 10$ $-24 \le k \le 25$ $-15 \le l \le 12$
R_{int}	0.0406	0.0709	0.0422	0.0795	0.0603
Independent reflections/ restraints/ parameters	3517/0/134	3666/0/138	3757/0/137	3867/0/137	3909/0/134
Refinement method	full-matrix least squares on F^2				
GOF on F^2	1.300	1.083	1.055	1.417	1.163
[a] R1, [b] wR_2 [I >2σ(I)] [a]	0.0266, 0.0739	0.0535, 0.1556	0.0230, 0.0347	0.0516, 0.1163	0.0303, 0.0665
R1, wR_2 (all data) [a]	0.0305, 0.0752	0.0626, 0.1620	0.0370, 0.0371	0.0620, 0.1193	0.0361, 0.0683

[a] $R_1 = \sum (||Fo| - |Fc||) / \sum |Fo|$; [b] $wR_2 = \sum w(|Fo|^2 - |Fc|^2)^2 / \sum w(|Fo|^2)^2]^{1/2}$

References

1. M. D. Segall, P. J. D. Lindan, M. J. Probert, C. J. Pickard, P. J. Hasnip, S. J. Clark and M. C. Payne, First-Principles Simulation: Ideas, Illustrations and the CASTEP Code, *J. Phys.: Condens. Matter*, 2002, **14**, 2717−2744.
2. J. P. Perdew, K. Burke and M. Ernzerhof, Generalized Gradient Approximation Made Simple, *Phys. Rev. Lett.*, 1996, **77**, 3865−3868.
3. M. J. Wang, X. R. Chen, Y. B. Tong, G. J. Yuan, X. M. Ren and J. L. Liu, Phase Transition, Dielectrics, Single-Ion Conductance, and Thermochromic Luminescence of an Inorganic–Organic Hybrid of [Triethylpropylammonium]-[PbI_3], *Inorg. Chem.*, 2017, **56**, 9525−9534.